ACS APPLIED MATERIALS & INTERFACES

www.acsami.org

Research Article

An Efficiency of 16.46% and a T_{80} Lifetime of Over 4000 h for the PM6:Y6 Inverted Organic Solar Cells Enabled by Surface Acid Treatment of the Zinc Oxide Electron Transporting Layer

Yunfei Han, Huilong Dong, Wei Pan, Bowen Liu, Xingze Chen, Rong Huang, Zhiyun Li, Fangsen Li, Qun Luo,* Jianqi Zhang,* Zhixiang Wei, and Chang-Qi Ma*

Cite This: https://doi.org/10.1021/acsami.1c02613

Read Online

ACCESS | Metrics & More | Article Recommendations | Supporting Information

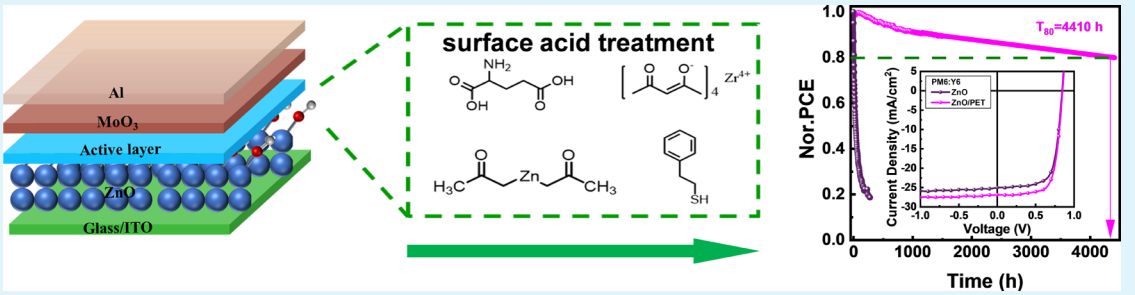

ABSTRACT: For the inverted organic solar cells (OSCs), the interface contacts between the ZnO electron transporting layer and the organic active layer play an important role in the device performance and stability. Since the solution-processed ZnO surface always contains some base or zinc salt contaminants, we explored how the surface pH conditions influence the performance and stability of the nonfullerene acceptor (NFA) cells. A tight relationship between the surface pH condition and the device performance and stability was established. Specifically, device performance and stability were improved by treating the ZnO films with acid solutions but worsened after base treatment. The large number of hydroxyl groups on the surface of the solution-processed ZnO films was proved to be the main reason for the surface pH condition-related performance, which caused oxygen-deficient defects and unfavorable vertical phase separation in the blend films, hindered the photogenerated charge transfer and collection, and consequently resulted in low short-circuit current density and power conversion efficiency (PCE). The surface −OH groups also boosted the photocatalytic activity and led to fast degradation of the nonfullerene acceptor. Removal of the surface −OH groups can alleviate such problems. Different acid solutions, ZrAcac, 2-phenylethylmercaptan (PET), and glutamic acid (GC), were used to treat the ZnO films, and PET treatment was the most effective treatment for performance improvement. An efficiency of 16.46% was achieved for the PM6:Y6 cells and the long-term stability under continuous illumination conditions was significantly improved with a T_{80} lifetime of over 4000 h (4410 h), showing the excellent long-term stability of this heterojunction solar cell. Our understanding of the surface pH condition-related device performance and stability would guide the development of a feasible method for solving the interface problems in OSCs. We also provide a practical strategy to modify ZnO with acid solutions for high-performance and stable NFA OSCs.

KEYWORDS: *organic solar cells, ZnO electron transporting layer, pH condition, surface passivation, long-term stability*

1. INTRODUCTION

Organic solar cells (OSCs) have emerged as a potential energy supply for wearable electronics and integrated photovoltaics due to the advantages of being lightweight, flexible, semi-transparent, and compatible with roll-to-roll printing.[1−3] In recent years, with the development of high-performance organic semiconductor materials, especially the nonfullerene acceptors (NFAs),[4,5] the highest performance of OSCs has exceeded 18%,[6,7] showing great potential in real applications. To push the real application of the OSCs, the reliability and the upscaling fabrication are an urgent demand. In the past 2 years, the PM6:Y6 solar cell was widely studied, and high efficiency was reported.[8] However, the stability was rarely reported yet.

In the inverted OSCs, ZnO is widely used as the electron transporting layer (ETL) owing to the good photoelectronic properties and low-temperature solution processability.[9]

Received: February 9, 2021
Accepted: March 31, 2021

Despite its excellent electron mobility and proper optical properties, solution-processed ZnO still faces several challenges in terms of high device performance. The solution-processed ZnO ETLs for the use of OSCs are usually fabricated from a colloidal route through a reaction between a base and Zn salts[10−12] or from a sol−gel method.[13,14] Whether it was fabricated by the nanoparticle route or the sol−gel route, the problem of ZnO ETLs almost originated from the surface ligands and surface defects.[15,16] These various surface defects would cause a high density of recombination centers, lead to insufficient charge transportation and extraction, and finally lower the power conversion efficiency of the OSCs.[17] The methods to solve this problem totally can be classified into two categories: using polar solvents,[18] hydrogen annealing,[19] or small molecules, like ethanedithiol,[20] phenols,[21] and glycine,[22] to remove the surface defects and using an extra layer[23,24] on top the ZnO films to passivate the defects. All these treatments would reduce the carrier recombination at the cathode interface and lead to remarkable enhancement of the short-circuit current and hence the device efficiency.[20−22]

In addition, the NFA-based OSCs were found to be more sensitive to the surface ligands of ZnO than the fullerene acceptor-based OSCs.[25,26] Due to the photocatalytic effect of the ZnO films, photochemical degradation of the organic materials dominated the degradation process for the NFA OSCs.[27] Several feasible strategies have been developed to improve the stability of NFA OSCs. Liu *et al.* utilized an organic conjugated small-molecule layer as a modifier of ZnO, and the overall performance and photostability of the NFA OSCs were improved.[28] Xu *et al.* developed the C_{60} self-assembled monolayer modifier for the ZnO ETL and reported[29] a lifetime of over 20 years (T_{80}) for PTB7-Th:IEICO-4F OSCs. In addition, Cheng *et al.*[30] demonstrated that potassium treatment of the sol−gel ZnO films induced vertical phase separation and improved the performance of the NFA OSCs. These works indicated that both the defect elimination and defect passivation categories are effective in improving the performance and stability of NFA OSCs. Although great breakthroughs in improving the efficiency and stability of NFA OSCs have been achieved by modifying the ZnO ETLs, the deep mechanism of surface treatment is not yet fully recognized in the previous studies. Therefore, systematically studying and fully understanding the influence of ZnO surface conditions on the device performance and stability and developing a general method to simultaneously improve the performance and stability are important.

We know that the surface characteristics of solution-processed ZnO films are determined by the synthesis conditions. Usually, the ZnO surface contains some base or zinc salt contaminants and dangling bonds. The stoichiometry of the base and zinc salts influences not only the crystallization of ZnO but also the surface potential of the NPs and consequently impacts the interface contact of the ETL and the photoactive layer. Thus, in this work, we first investigated the effect of surface pH conditions on the performance and stability of OSCs by treating the ZnO films with an acid and a base. We found that the presence of a large number of hydroxyl groups at the ZnO/active layer interface is the main reason for the inferior performance and poor stability. The performance and stability were improved with the removal of hydroxyl groups by treating the ZnO films with several kinds of acidic solutions. We chose different acidic materials, *i.e.*, zinc acetate ($Zn(OAc)_2$), zirconium acetylacetonate (ZrAcac), glutamic acid (GC), and 2-phenylethylmercaptan (PET), to treat the ZnO films. Among them, PET showed an overwhelming effect in improving the long-term stability of NF OSCs. For the devices based on poly[[4,8-bis[5-(2-ethylhexyl)-4-fluoro-2-thienyl]benzo[1,2-*b*:4,5-*b*′]dithiophene-2,6-diyl]-2,5-thiophenediyl[5,7-bis(2-ethylhexyl)-4,8-dioxo-4*H*,8*H*-benzo-[1,2-*c*:4,5-*c*′]dithiophene-1,3-diyl]-2,5-thiophenediyl] (PM6) as a polymer donor and (2,20-((2*Z*,20*Z*)-((12,13-bis(2-ethylhexyl)-3,9-diundecyl-12,13-dihydro-[1,2,5]thiadiazolo-[3,4-*e*]thieno[2″,30′:4′,50]thieno[20,30:4,5]pyrrolo[3,2-*g*]-thieno[20,30:4,5]thieno[3,2-*b*]indole-2,10-diyl)bis-(methanylylidene))bis(5,6-difluoro-3-oxo-2,3-dihydro-1*H*-indene-2,1-diylidene))dimalononitrile) (Y6) as an electron acceptor, the PCE was boosted from 14.71 to 16.46%. The long-term stability during continuous illumination was greatly improved compared with pristine ZnO-based OSCs, showing a lifetime (T_{80}) of over 4000 h. This work gives deep insight into the ZnO surface pH condition-dependent OSC performance and degradation and provides a universal defect elimination method through surface acid treatment to achieve high efficiency and long-term stability for the inverted NFA OSCs. This work also shows the excellent long-term stability of the PM6:Y6 inverted solar cells with a surface acid-treated ZnO ETL.

2. EXPERIMENTAL SECTION

2.1. Materials. PM6, PM7, IT-4F, and Y6 were purchased from Solarmer Materials Inc., Beijing. PET, $Zn(OAc)_2$, TMAH, and chlorobenzene (CB, 99.8%) were purchased from J&K Scientific Ltd. 1,8-Diiodooctane (DIO) and 1-chloronaphthalene (CN) were purchased from Sigma-Aldrich.

2.2. The Synthesis and Modification of ZnO ETLs. ZnO nanoparticles (NPs) with a size around 4 nm were synthesized through the reaction between Zn acetate and tetramethylammonium hydroxide (TMAH) in a DMSO solvent as reported by Qian *et al.*[31] Specifically, Zn acetate was dissolved in dimethyl sulfoxide (DMSO), and TMAH was dissolved in ethanol as well. After that, the ZnO NPs were dispersed in ethanol with a concentration of 10 mg/mL. The ZnO electron transporting layer was fabricated by spin-coating the ZnO NP inks at 3000 rpm for 1 min, followed by annealing at 120 °C for 10 min in the N_2-filled glove box. For the modification of ZnO ETLs by $Zn(OAc)_2$ solution, $Zn(OAc)_2$ was first dissolved in methanol with weight concentrations of 1, 5, and 10 mg/mL. Then, the $Zn(OAc)_2$ solution was dropped onto the ZnO films and spread out through spin coating at 3000 rpm for 30 s. For the treatment of ZnO ETLs by TMAH solution, TMAH was first dissolved in methanol with concentrations of 1, 2, and 4 mg/mL. After that, the TMAH solution was dropped onto the ZnO ETL and spread out through spin coating at 3000 rpm for 30 s. For the modification of ZnO ETLs by PET, PET was first dissolved in methanol with concentrations of 0.1, 0.5, and 1 vol %, and such solution was dropped onto the ZnO films and kept for 5 s. After that, the residual PET solution was spread out through spin coating with a speed of 3000 rpm for 30 s. For the modification of ZnO ETLs by ZrAcac solution, ZrAcac was first dissolved in chloroform with a weight concentration of 0.5 mg/mL. Then, the ZrAcac solution was dropped onto the ZnO films and spread out through spin coating at 3000 rpm for 30 s. For the modification of ZnO ETL by GC solution, GC was first dissolved in methanol with a weight concentration of 1 mg/mL. Then, the GC solution was filtered and dropped onto the ZnO films and spread out through spin coating at 3000 rpm for 30 s. All the modified ZnO ETLs were annealed at 120 °C for 5 min in the N_2-filled glove box.

2.3. The OSC Fabrication. Inverted OSCs with a structure of ITO/ZnO/active layer/MoO_3/Al were fabricated. After UV ozone treatment of the ITO substrates for 30 min, ZnO electron transporting layers were deposited on the ITO electrodes by spin-

https://doi.org/10.1021/acsami.1c02613
ACS Appl. Mater. Interfaces XXXX, XXX, XXX−XXX

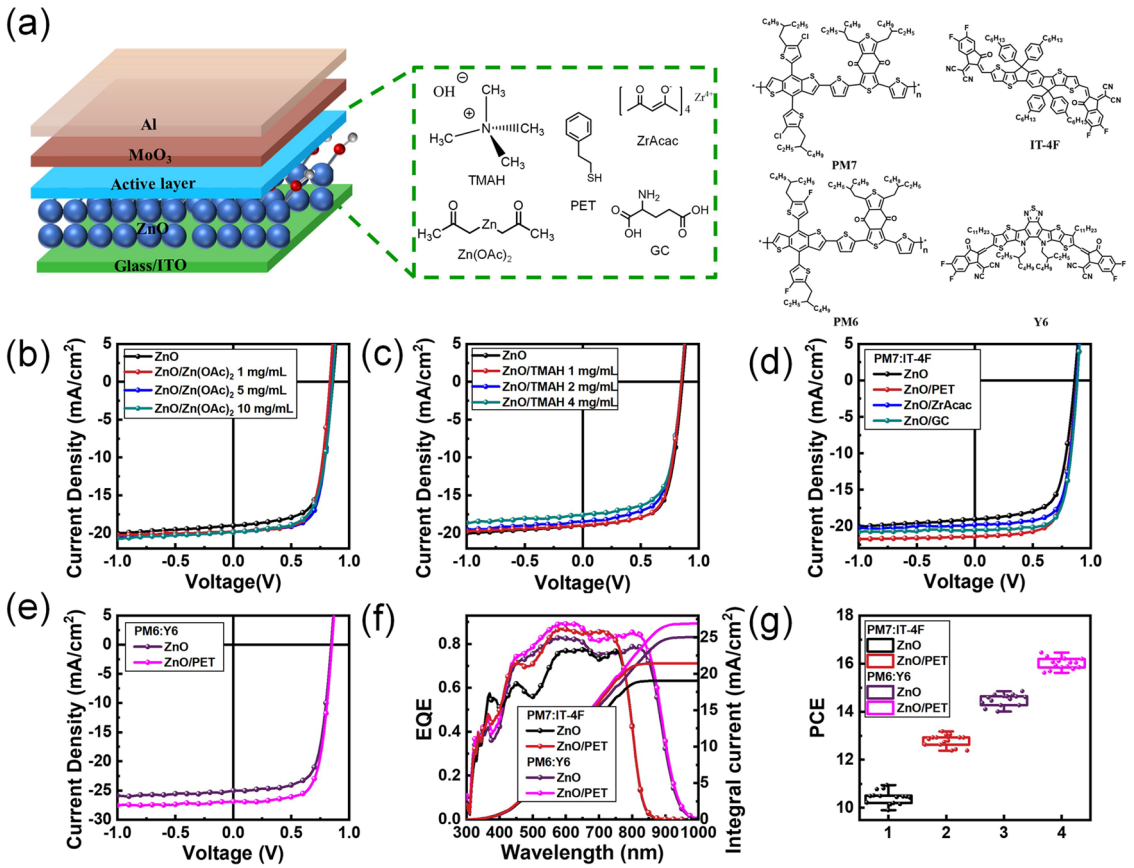

Figure 1. (a) Device structure of the inverted organic solar cells and the molecular structure of TMAH, $Zn(OAc)_2$, PET, ZrAcac, GC, the organic donor PM7, PM6, the acceptor IT-4F, and Y6. (b, c) $J-V$ characteristics with $Zn(OAc)_2$- and TMAH-treated ZnO as the ETLs and (d, e) $J-V$ characteristics of the PM7:IT-4F and PM6:Y6 solar cells with different ZnO ETLs. (f) EQE spectra of PM7:IT-4F and PM6:Y6 solar cells with ZnO and PET-treated ZnO ETLs. (g) Histogram of the device performance of the PM7:IT-4F and PM6:Y6 solar cells with ZnO and PET-treated ZnO as the ETLs.

coating the ZnO inks at 2500 rpm for 60 s and annealed at 120 °C for 10 min in the N_2-filled glove box. Then, the ZnO ETL was treated with PET, $Zn(OAc)_2$, ZrAcac, or TMAH. Then, the active layers (PM6:Y6 and PM7:IT-4F) were spin-coated from a mixed solution of polymer donors and nonfullerene acceptors. For the PM6:Y6 solar cells, the mixed solution of PM6 and Y6 together with 0.5 vol % CN was dissolved in CF with concentrations of 7 and 8.4 mg/mL, respectively. For the PM7:IT-4F solar cells, the mixed solution of PM7 and IT-4F was dissolved in CB with concentrations of 10 and 10 mg/mL, respectively. In addition, DIO was added as an additive with a concentration of 0.5 vol % as well. The active layers were fabricated by spin-coating the precursor solution at 2000 rpm for 1 min and annealed at 100 °C for 10 min. Finally, 10 nm MoO_3 and 200 nm Al were successfully thermally deposited successively on top of the active layers at a vacuum level below 1×10^{-4} Pa. The effective areas of the devices were 0.09 cm^2.

2.4. Characterization. The electrochemical impedance spectra were measured using an Autolab electrochemical workstation (Autolab PGSTAT 302N, Metrohm Autolab B.V.) at frequencies from 2 MHz to 1000 Hz under dark conditions. The XPS spectra of ZnO with different modifications were measured using an ESCALAB 250Xi spectrometer with a monochromatic Al Kα X-ray source with an overall energy space of ΔE = 0.1 eV. The contact angle between ZnO and solvents was recorded by a contact angle meter model SL150 (USA KINO Industry). The UV−vis−NIR spectra of the films were measured by a Lambda 750 UV/vis/NIR spectrophotometer (PerkinElmer). The photoluminescence spectra of the ZnO films were recorded by a Hitachi F4600 fluorescence spectrophotometer. Grazing incidence wide-angle X-ray scattering (GIWAXS) of the active layers was measured by the XEUSS SAXS/WAXS system (Xenocs, France). ToF-SIMS of the devices was carried out using a TOF.SIMS5-100. The atomic force microscopy images of the films of ZnO were studied using a Veeco Dimension 3100 instrument at the ambient temperature in tapping mode. The current density−voltage ($J-V$) measurements were carried out in a nitrogen glove box with a Keithley 2400 source meter under a Newport solar simulator (100 mW/cm^2). External quantum efficiencies (EQEs) were measured under simulated one sun operation conditions with light from a 150 W tungsten halogen lamp (Osram 64610) as the probe light, a monochromator (Zolix, Omni-λ300) for selecting the wavelength, and an $I-V$ converter for recording the response. Light illuminated the sample *via* a small aperture with a radius of 1.5 nm, and a calibrated Si cell was used as a reference. The long-term stability of the devices was recorded through period $J-V$ sweeps under continuous illumination in the N_2-filled glove box.

3. RESULTS AND DISCUSSION

Herein, ZnO NPs were synthesized using the coprecipitation method through the reaction between zinc acetate $Zn(OAc)_2$ and tetramethylammonium hydroxide (TMAH) in the solvent of dimethyl sulfoxide (DMSO) and ethanol following a similar route as that reported by Qian *et al.*[15] The obtained ZnO NPs have a wurtzite structure as shown in the XRD patterns (Figure S1a). The NPs showed a crystal size of approximately 4 nm and exhibited good dispersibility in the ethanol solvent, as shown in the high-resolution transmission electron microscopy (HR-TEM) images (Figure S1b). To investigate the effect of acid and base treatment of the ZnO films on the performance

https://doi.org/10.1021/acsami.1c02613
ACS Appl. Mater. Interfaces XXXX, XXX, XXX−XXX

Table 1. Performance Parameters of the PM7:IT-4F Inverted Solar Cells with Pristine ZnO and $Zn(OAc)_2$- and TMAH-Treated ZnO Films as ETLs[a]

ETL	concentration [mg/mL]	V_{OC} [V]	J_{SC} [mA/cm^2]	FF	PCE [%]
ZnO	w/o	0.86	19.02	0.67	10.95
		0.86 ± 0.01	18.37 ± 0.54	0.66 ± 0.01	10.43 ± 0.28
ZnO/$Zn(OAc)_2$	1	0.86	19.21	0.69	11.40
		0.86 ± 0.01	18.76 ± 0.65	0.68 ± 0.01	10.97 ± 0.34
	5	0.86	19.13	0.72	11.85
		0.86 ± 0.01	19.10 ± 0.21	0.71 ± 0.01	11.66 ± 0.26
	10	0.86	19.87	0.67	11.45
		0.86 ± 0.01	19.52 ± 0.34	0.67 ± 0.01	11.25 ± 0.14
ZnO/TMAH	1	0.85	18.80	0.68	10.87
		0.85 ± 0.01	18.73 ± 0.11	0.68 ± 0.01	10.83 ± 0.03
	2	0.85	18.47	0.65	10.20
		0.85 ± 0.01	18.42 ± 0.13	0.65 ± 0.01	10.17 ± 0.08
	4	0.85	17.58	0.66	9.86
		0.85 ± 0.01	17.50 ± 0.05	0.65 ± 0.02	9.67 ± 0.28

[a]Calculated from 15 individual devices.

Table 2. Performance Parameters of the PM7:IT-4F and PM6:Y6 Inverted Solar Cells with Different ZnO ETLs[a]

active layer	ETL	V_{OC} [V]	J_{SC} [mA/cm^2]	FF	PCE [%]
PM7:IT-4F	ZnO	0.86	19.02	0.67	10.95
		0.86 ± 0.01	18.37 ± 0.54	0.66 ± 0.01	10.43 ± 0.28
	ZnO/PET	0.88	21.41	0.70	13.19
		0.87 ± 0.01	21.00 ± 0.31	0.70 ± 0.01	12.79 ± 0.25
	ZnO/ZrAcac	0.88	19.77	0.72	12.53
		0.87 ± 0.01	19.70 ± 0.08	0.71 ± 0.01	12.18 ± 0.26
	ZnO/GC	0.88	20.54	0.72	13.01
		0.87 ± 0.01	20.48 ± 0.16	0.72 ± 0.01	12.82 ± 0.20
PM6:Y6	ZnO	0.84	25.02	0.70	14.71
		0.84 ± 0.01	24.97 ± 0.31	0.69 ± 0.01	14.47 ± 0.15
	ZnO/PET	0.85	26.89	0.72	16.46
		0.85 ± 0.01	26.76 ± 0.27	0.71 ± 0.01	16.15 ± 0.35

[a]Calculated from 15 individual devices.

and stability of the OSCs, ZnO films treated with $Zn(OAc)_2$ and TMAH solutions were used as the ETLs of the inverted OSCs. First, we ensured that neither $Zn(OAc)_2$ nor TMAH treatment destroyed the ZnO films based on the absorbance spectra (Figure S1c). Then, a series of devices with the inverted structure of ITO/ZnO/active layer/MoO_3/Al (as shown in Figure 1a) were fabricated. First, a PM7:IT-4F device was fabricated. The molecular structures of $Zn(OAc)_2$, TMAH, the organic donor PM7, and the acceptor IT-4F are shown in this figure too. The treatment of ZnO films was carried out as follows: $Zn(OAc)_2$ and TMAH solutions with different concentrations were dissolved in methanol to form solutions and spin-coated on top of ZnO films. The device performance is shown in Figure 1b,c, and the corresponding performance parameters are listed in Table 1. The device with a pristine ZnO ETL and a PM7:IT-4F active layer presented an open-circuit voltage (V_{OC}), a short-circuit current (J_{SC}), a fill factor (FF), and a power conversion efficiency (PCE) of 0.86 V, 19.02 mA/cm^2, 67%, and 10.95%, respectively. With $Zn(OAc)_2$ treatment, the device performance gradually improved with increasing $Zn(OAc)_2$ concentration from 1 to 10 mg/mL, with saturation at 5 mg/mL. With optimization, the best PCE of 11.85% with a V_{OC} of 0.86 V, a J_{SC} of 19.13 mA/cm^2, and an FF of 72% was obtained. In contrast, the TMAH treatment of ZnO films caused negative effects on the device performance. With increasing TMAH concentration from 1 to 4 mg/mL, a gradual decrease in performance was observed. Particularly, after treatment with 4 mg/mL TMAH solution, the device only gave a PCE of 9.86%, with V_{OC}, J_{SC}, and FF of 0.85 V, 17.58 mA/cm^2, and 66%, respectively. In addition, the device with the TMAH-treated ZnO ETL showed a typical "light soaking" issue: several minutes of white light soaking was needed to achieve normal $J-V$ characteristics. Taking the device with the 2 mg/mL TMAH-treated ZnO film ETL as an example, the evolution of the J-V characteristics during 10 min of illumination is presented in Figure S2. As shown in Figure S2, the fresh device showed an obvious "S"-shaped $J-V$ curve. During continuous light soaking of 10 min, such an abnormal $J-V$ curve gradually transformed to the normal curve. Correspondingly, the device performance increased from 5.88 to 10.03%. The light soaking issue of the inverted OSCs with ZnO or TiO_2 ETLs has been ascribed to the low electron mobility of these ETLs because of various defects.[32] For metal oxide NPs, the surface defects usually originate from surface ligands and the remaining reactants. Among them, the surrounding hydroxyl groups introduced by base reactants could be captured by oxygen vacancies and form charge recombination centers, consequently aggravating electron accumulation at the cathode.[33] Therefore, it is reasonable that treatment of ZnO films with high-concentration base solutions resulted in a serious light soaking issue

https://doi.org/10.1021/acsami.1c02613
ACS Appl. Mater. Interfaces XXXX, XXX, XXX−XXX

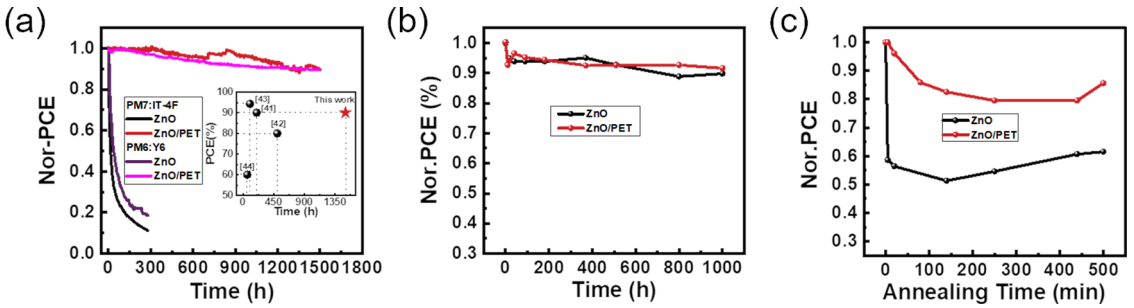

Figure 2. (a) PCE decay of the PM7:IT-4F and PM6:Y6 inverted solar cells with the pristine ZnO and PET-treated ZnO ETLs (the inset is the comparison of the stability of the devices presented in this work with those of previously reported PM6:Y6 OSCs). (b) Storage stability of the PM6:Y6 devices with ZnO and PET-treated ZnO ETLs in air with a relatively fixed humidity from 20 to 30%. (c) Thermal stability of the PM6:Y6 OSCs with ZnO and PET-treated ZnO as the ETLs under 80 °C continuous annealing.

since more hydroxyl groups would be introduced on top of the ZnO films.

Based on the above results, it was reasonable to speculate that the inferior performance of the pristine ZnO ETL-based solar cells is highly related to the residual hydroxyl groups on the ZnO films, and acid treatment of the ZnO ETL seems to be a practical route for solving this problem. Considering this, we chose several different acids, 2-phenylethylmercaptan (PET), ZrAcac, and glutamic acid (GC), which are a typical protonic acid, Lewis acid, and organic acid, respectively, to treat the ZnO films and investigate the generality. The molecular structures of these acids are shown in Figure 1a. The pristine ZnO and acid-treated ZnO films were used as the ETLs for the PM7:IT-4F OSCs. Figure 1d shows the current density versus voltage ($J-V$) characteristics of these devices, and the device performance of these cells using acid-treated ZnO ETLs is shown in Table 2. To exclude the influence of the solvents, methanol-treated ZnO films were also used as ETLs for comparison, and the performance is shown in Table S1. As shown in Table 2, compared with the pristine ZnO ETL-based devices, the acid-treated ZnO ETL devices exhibited better device performance. The device with the ZrAcac-treated ZnO ETL presented V_{OC}, J_{SC}, FF, and PCE of 0.88 V, 19.77 mA/cm^2, 72%, and 12.53%, respectively. The device with the GC-treated ZnO ETL presented V_{OC}, J_{SC}, FF, and PCE of 0.88 V, 20.54 mA/cm^2, 72%, and 13.01%, respectively. Among them, the device with the PET treated-ZnO ETL showed the most effective performance improvement and a significantly improved efficiency of 13.19%, and V_{OC}, J_{SC}, and FF of 0.88 V, 21.41 mA/cm^2, and 70%, respectively, were observed. Compared to the pristine ZnO ETL-involved devices, the treatment of ZnO ETLs by these acidic solutions prompted an obvious increase in J_{SC}. As shown in Figure 1f, the integrated current density calculated over the EQE spectra was in good agreement with the $J-V$ characteristics.

The recently popularly studied PM6:Y6 heterojunction solar cells, which are possible to reach an efficiency of over 16%,[34−36] were also fabricated. Similar to the PM7:IT-4F solar cells, synergistic improvements in the efficiency were observed in the PM6:Y6 heterojunction solar cells. Figure 1e,f shows the $J-V$ characteristics and EQE spectra of the PM6:Y6 devices with pristine ZnO and PET-treated ZnO ETLs. As shown in Table 2, the PM6:Y6 devices with pristine ZnO ETLs showed the highest PCE of 14.71%, with a V_{OC} of 0.84 V, a J_{SC} of 25.02 mA/cm^2, and an FF of 70%. With PET-treated ZnO as the ETL, the highest performance increased from 14.71 to 16.46%, with a V_{OC} of 0.85 V, a J_{SC} of 26.89 mA/cm^2, and an FF of 72%. The best performance of the PM6:Y6 device with the PET treated-ZnO ETL is among the highest efficiencies for these material-involved OSCs.[8,30,34,37−39] Moreover, the influence of the methanol solvent could be excluded due to the poor performance of the device when the ZnO film was treated with the methanol solvent, as presented in Table S1. Figure 1g shows histograms of the PM7:IT-4F and PM6:Y6 device performance of 15 individual cells with pristine ZnO and PET-treated ZnO ETLs. The device with the PET-treated ZnO ETL has a much higher average performance. Specifically, for the PM7:IT-4F and PM6:Y6 devices with PET-treated ZnO ETLs, at least 50% of the devices gave efficiencies exceeding 13.0 and 16.0%, respectively.

In addition to the enhancement in the device performance, the use of a PET-treated ZnO ETL also significantly improved the long-term photostability of the inverted solar cells. The long-term photostability of the unencapsulated ZnO and PET-treated ZnO ETL-based OSCs was investigated in a N_2-filled glove box under continuous illumination at the maximal power point. The evolution of the device performance is exhibited in Figure 2a and performance parameters of the fresh devices with ZnO and PET-treated ZnO as the ETLs are shown in Table 1. The PM7:IT-4F devices with the pristine ZnO ETL degraded quickly during 100 h of continuous illumination. Regarding the PM6:Y6 devices, the pristine ZnO ETL device quickly degraded within 300 h, whereas the PET-treated ZnO OSC exhibited excellent long-term stability, retaining 90% of the initial efficiency after 1500 h of continuous illumination. For the PM7:IT-4F device, the increase in PCE at around 900 h was due to the variation of the lamp intensity due to the equipment reason. The lifetime of the cells (T_{80}) was estimated through the extension of the decay curves after the burn-in step (Figure S3) and lifetimes of approximately 2700 and 4410 h were obtained for the PM7:IT-4F and PM6:Y6 solar cells, respectively. The quick degradation of the PM6:Y6 binary solar cells had been reported in a previous work.[40] Herein, as shown in the inset of Figure 2a, the lifetime value of both the PM7:IT-4F and PM6:Y6 OSCs was among the longest values for these two photoactive systems as far as we knew.[41−46] The influence of PET treatment on the air stability was investigated by comparing the stability of the ZnO and PET-treated ZnO ETL-based unencapsulated OSCs in air with a relatively fixed humidity from 20 to 30%. As shown in Figure 2b, the PET-treated cells had a similar stability to the control one. Both of them showed excellent stability, retaining about 90% of initial PCE after 1000 h. This result indicated that the

https://doi.org/10.1021/acsami.1c02613
ACS Appl. Mater. Interfaces XXXX, XXX, XXX−XXX

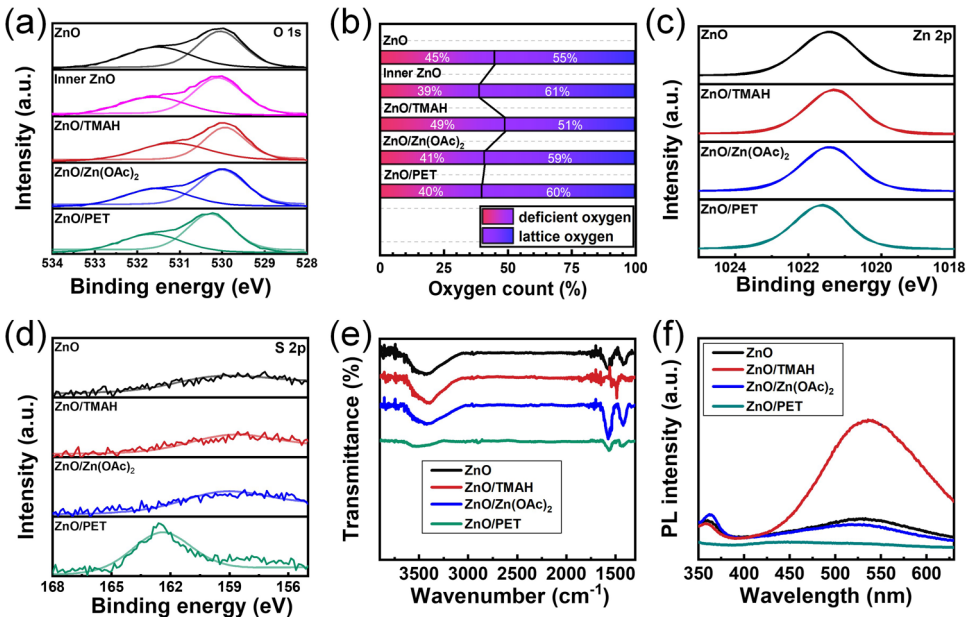

Figure 3. (a) XPS spectra of the O 1s core level, (b) percentage of deficient oxygen and lattice oxygen in different ZnO films, and XPS spectra of (c) Zn 2p and (d) S 2p core levels in different ZnO films. (e) FT-IR spectra and (f) PL spectra of different ZnO films.

light-induced photocatalytic effect of ZnO might be the main reason for interface degradation between ZnO and the active layer. In the case of storage stability of these devices, less influence by the ZnO ETL was found either in air condition or in the nitrogen-filled glove box. The thermal stability test of PM6:Y6 OSCs was also investigated under 80 °C continuous annealing for 500 min at an N_2-filled glove box. As shown in Figure 2c, the devices with PET-treated ZnO ETLs exhibited excellent thermal stability, retaining above 85% of the initial PCE after 500 min, while the control one retained 60% of the initial PCE. These stability results under continuous illumination condition strongly proved that the PM6:Y6 solar cells could be quite stable as the interface degradation issue was solved, which is encouraging for their real application.

The dark $J-V$ characteristics, electrochemical impedance spectra (EIS), and V_{OC} *vs* light intensity were investigated and carefully analyzed to study the trap states and diode performance of the devices with pristine ZnO and PET-treated ZnO films. From the dark $J-V$ characteristics of the devices (Figure S4a), an increased rectification ratio from 3.3 $\times$ 10^2 for the pristine ZnO-based device to 1.6 $\times$ 10^4 for the device with the PET-treated ZnO ETL was observed. It indicated improved charge selectivity of the device with the PET-treated ZnO ETL, which would lead to an improvement in FF. In the Nyquist plots of these devices (Figure S4b), all the plots exhibited asymmetric semicircles that could be fitted with the equivalent circuit model (as shown in the inset of Figure S4b) that comprised of three resistances R_s (series resistance), R_{trans} (transport resistance), and R_{rec} (recombination resistance) and two capacitances C_{trans} and C_{rec}. The fitting parameters are summarized in Table S2 (Supporting Information). For the pristine ZnO-based solar cells, R_s, R_{trans}, R_{rec} and C_{trans} and C_{rec} were 41, 856, and 144 ohm and 1.3 $\times$ 10^{-8} and 1.1 $\times$ 10^{-8} F, respectively. For the PET-treated ZnO-involved solar cells, R_s, R_{trans}, and R_{rec} and C_{trans} and C_{rec} are 41, 475, 127 ohm and 1.7 $\times$ 10^{-8} and 1.2 $\times$ 10^{-8} F, respectively. Compared with the pristine ZnO-based solar cells, the devices with the PET-treated ZnO ETL displayed similar R_s and R_{rec} but smaller R_{trans}. These results suggested that PET-treated solar cells possessed better electrical properties with easier carrier transport.[38,47] The light intensity-dependent V_{OC} and J_{SC} of these devices are shown in Figure S4c,d. Regarding the light intensity dependence of J_{SC} for these devices, all the J_{SC} values were linearly correlated with the light intensity with slopes of approximately 0.92 and 0.94 for the solar cells. Theoretically, J_{SC} is light intensity-dependent with a relationship of $J \propto I^{\alpha}$, where α usually ranges from 0.85 to 1 for OSCs,[48,49] and α close to 1 means less carrier loss through bimolecular recombination and space charge effects. Otherwise, higher carrier loss occurs if α is much smaller than 1. Therefore, this result indicated negligible bimolecular recombination and space charge effect in all the devices. Regarding the light intensity-dependent V_{OC}, a correlation between V_{OC} and the light intensity is expected with a slope as nK_BT/q, where n, K_B, T, and q are the ideal factor, Boltzmann constant, absolute temperature, and elementary charge, respectively.[50] As shown in Figure S4d, slopes of $1.22K_B/q$ and $1.07K_B/q$ were estimated for the solar cells with pristine ZnO and PET-treated ZnO ETLs. The larger slope of the pristine ZnO-based solar cells than the PET-treated ZnO-based device indicated that more trap-assisted recombination existed.[50] Since the device layers were the same in these solar cells except for the ZnO ETL, the existence of defect-assisted recombination was ascribed to recombination at the interface of ZnO and the organic layer in the pristine ZnO-based solar cells.

With the improved performance in hand, we further systematically explored the deep mechanism of acid treatment from four different aspects, *i.e.*, the structure, photoelectronic properties of the ZnO layer, the variation of morphology, and vertical phase separation component of the organic photoactive layer. First, the change in the structure and components of the ZnO films after surface modification was investigated. The X-ray photoelectron spectroscopy (XPS) spectra of the O 1s, Zn 2p, and S 2p core levels for the initial ZnO films and $Zn(OAc)_2$-, TMAH-, and PET-treated ZnO films were

https://doi.org/10.1021/acsami.1c02613
ACS Appl. Mater. Interfaces XXXX, XXX, XXX−XXX

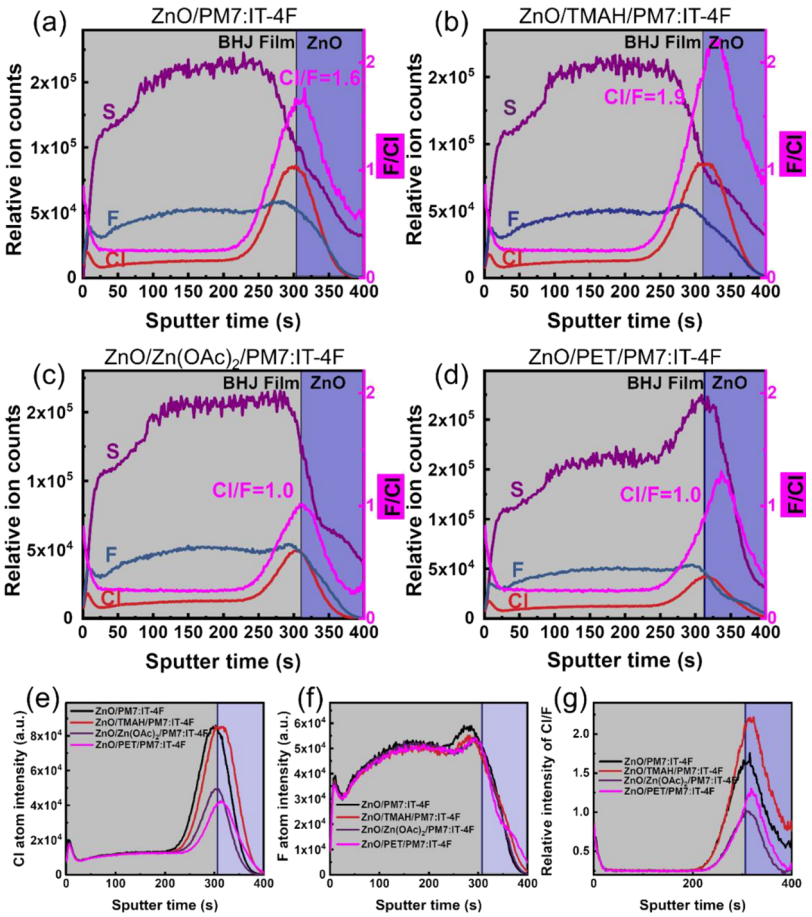

Figure 4. (a–d) ToF-SIMS depth profiles of the PM7:IT-4F films, the intensity of (e) Cl atoms and (f) F atoms, and (g) relative ratio of Cl/F in PM7:IT-4F films on top of the pristine ZnO and TMAH-, $Zn(OAc)_2$-, and PET-treated ZnO film ETLs.

measured and are shown in Figure 3a–d. Figure 3a shows that the core level of the O 1s spectra for these films is composed of two peaks. The peaks centered at 530 and 532.0 eV were from lattice oxygen and defect oxygen, respectively.[13] The oxygen defects include oxygen vacancy and surface-absorbed oxygen from the contaminants, such as hydroxy groups. To identify the origin of oxygen defects, the XPS spectra of the inner ZnO films were also detected by etching the ZnO films. The curves showed an obvious decrease in O 1s peaks at 532.0 eV, indicating much fewer oxygen defects from absorbed contaminants. In comparison with the pristine ZnO films, the position of the peaks of O 1s and Zn 2p core levels for the $Zn(OAc)_2$-treated ZnO films did not change, but the binding energy location for the TMAH- and PET-treated ZnO films slightly changed, which indicated that the electronic structure of ZnO films was affected by the organic molecules TAMH and PET. The relative intensity of the peaks at 530 eV for $Zn(OAc)_2$- and PET-treated ZnO films was stronger than that for the pristine ZnO films, indicating that the amount of lattice oxygen increased and more Zn atoms were bound to the O atoms. Meanwhile, the ratio of defect oxygen to lattice oxygen was calculated and is shown in Figure 3b. In the pristine ZnO films, the ratio was 0.45. With TMAH treatment, the ratio increased to 0.49, while $Zn(OAc)_2$ and PET treatment caused the decrease in the values to 0.41 and 0.40, respectively. This might be further explained as follows: the absorbed oxygen from hydroxyl groups could be effectively removed through treatment with acid solutions, whereas the lattice oxygen and vacancy oxygen remained in the films. Therefore, after surface acid treatment, a relatively constant ratio of defect oxygen to lattice oxygen of about 0.4 was observed, which was nearly in agreement with the ratio of the inner films. In addition, Figure 3d shows that the PET-treated ZnO films contained a peak at 162.5 eV that could be ascribed to the −SH groups in PET.[51−53] The appearance of a peak from −SH groups indicated the existence of PET in these films. Figure 3e shows the Fourier-transformed infrared spectroscopy (FT-IR) results of the films. For all these films, the peaks at 3000 cm^{-1} were attributed to the stretching modes of the surface −OH groups, and peaks at 1500 and 1200 cm^{-1} were from the asymmetric and symmetric stretching modes of the −COO group, respectively. The observation of −OH and −COO groups indicated that the residual acetate groups from TMAH and $Zn(OAc)_2$ were not completely removed from the ZnO NPs. The intensity of the carboxyl group peaks at 1500 and 1200 cm^{-1} increased for the $Zn(OAc)_2$-treated ZnO films, while it decreased in the TMAH- and PET-treated films. From the intensity of the peaks at approximately 3000 cm^{-1}, we found that treatment of the ZnO films with TMAH led to more residual hydroxyl groups, while $Zn(OAc)_2$ and PET treatment caused an obvious decrease. Therefore, the FT-IR results, together with the XPS spectra, proved that surface acid treatment has removed the surface hydroxyl groups. Based on performance improvement with acid-treated ZnO ETLs, a tight correlation between the content of surface hydroxyl groups and the performance could be established.

https://doi.org/10.1021/acsami.1c02613
ACS Appl. Mater. Interfaces XXXX, XXX, XXX−XXX

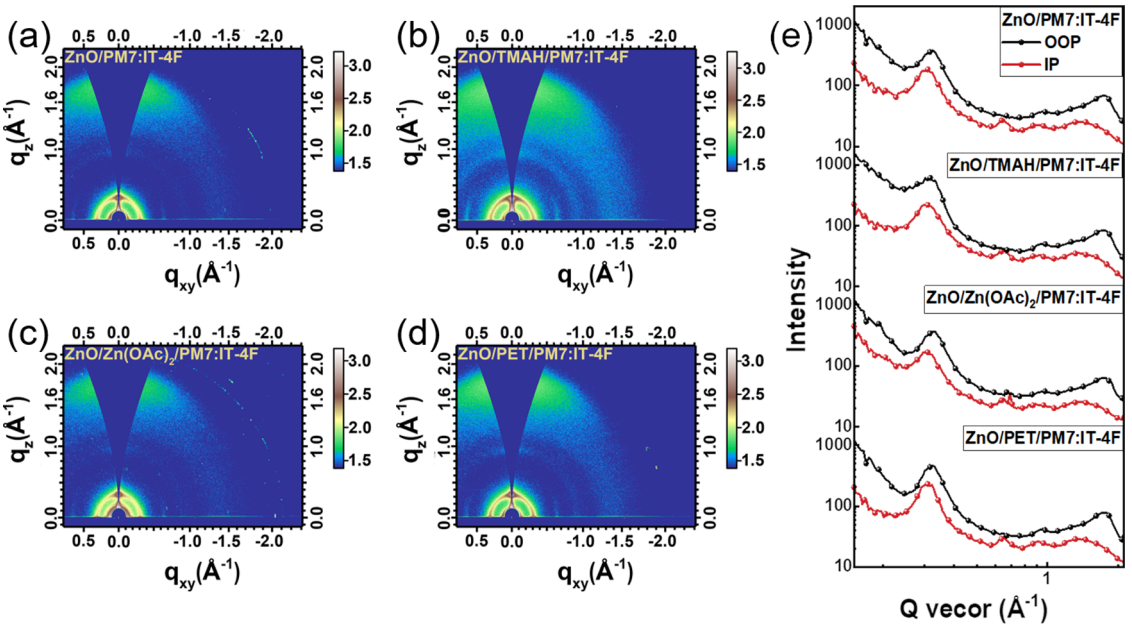

Figure 5. (a–d) GIWAXS 2D scattering pattern images and (e) line profiles of the PM7:IT-4F films on top of ZnO and TMAH-, $Zn(OAc)_2$-, and PET-treated ZnO films.

Second, the influence of acid and base treatment on the photoelectrical properties of the ZnO films was studied through photoluminescence (PL) spectroscopy. The PL spectra (Figure 3f) of the ZnO and treated ZnO films revealed an obvious intensity decrease after PET treatment. Excited at 320 nm, these films showed a typical green emission peak centered at around 530 nm and a weak blue emission peak centered at around 380 nm. The emission peaks at 530 and 380 nm originate from oxygen defect-related and band edge emissions, respectively.[54,55] The $Zn(OAc)_2$- and PET-treated ZnO films showed a sharp decrease in the emission intensities at 530 nm. Since the ZnO films have similar film thicknesses, the dramatic decrease in the 530 nm emission for the PET-treated ZnO films suggested the decrease of oxygen defects, which was proved by the XPS spectra. In contrast, the TMAH-treated ZnO film showed stronger PL emission at approximately 530 nm.

Third, we know that the surface energy and surface morphology of the underlying buffer layers play a significant role in the phase separation, vertical composition, crystallinity, and molecular orientation of organic blend films.[56−58] Therefore, the surface morphology and surface energy of the ZnO and treated ZnO films were investigated. As shown in the atomic force microscopy (AFM) images of the ZnO films in Figure S5, the pristine ZnO and treated ZnO films showed similar morphologies and surface roughness. For example, the root mean square roughness (RMS) values of the pristine ZnO and PET-treated ZnO films were 3.10 and 3.24 nm, respectively, suggesting that the surface treatment did not cause a large change in the surface roughness. Then, the surface energy of different ZnO films was studied by testing the contact angle, and images of a drop of water/diiodomethane (DIM) on top of ZnO and TMAH-, $Zn(OAc)_2$-, and PET-treated ZnO films are exhibited in Figure S6. The contact angles of water on top of different ZnO films were 31.11°, 23.60°, 34.93°, and 55.99°, respectively. The contact angles of DIM on top of different ZnO films were 25.54°, 20.23°, 24.57°, and 20.49°, respectively. The surface energies (γ_{total}) of the ZnO and TMAH-, $Zn(OAc)_2$-, PET-treated ZnO films were calculated to be approximately 65, 69, 63, and 54 mN/m based on the Owens−Wendt−Rabel−Kaelble (OWRK) method, respectively.[59] This observation demonstrated that the PET-treated ZnO films were more hydrophobic than the other films. Meanwhile, the values of γ_{polar} and $\gamma_{dispersive}$ were obtained from the water and DIM contact angles of different ZnO films. The calculated γ_{polar} values of ZnO and TMAH-, $Zn(OAc)_2$-, and PET-treated ZnO films were approximately 32, 35, 29, and 14 mN/m, respectively. The ZnO films were more polar owing to the excess of −OH groups. The γ_{polar} of the acid-treated ZnO films was smaller, indicating the removal of −OH groups.

Fourth, the time-of-flight secondary ion mass spectrometry (ToF-SIMS) images of the films were obtained to investigate the changes in the vertical components of the devices. Because of the existence of F and Cl in PM7 and IT-4F, the contents of the donor and acceptor could be determined from the contents of Cl and F atoms in the blend films. Thus, PM7:IT-4F blend films were chosen herein. Figure 4a–g shows the depth profiles of PM7:IT-4F films on different ZnO films. To clearly show the component difference in these films, the change of Cl and F and intensity ratios of Cl to F in the four films are exhibited in Figure 4e–g. We found that the content of F in these films was nearly the same, while the content of Cl was different, especially at the ZnO/BHJ interface. A sharp peak of Cl at the ZnO/BHJ interface was observed, implying more donors at the interface. The enrichment of polymer at the ZnO interface might be due to the stronger interaction effect between PM7 and ZnO and the poor miscibility of PM7 and IT-4F, which would cause pre-aggregation at the bottom layer.[60] Density functional theory (DFT) simulation (Figure S8) showed a much stronger binding energy between donors and ZnO (6.79 eV) than the binding energy between the acceptor and ZnO (1.70 eV) when enormous hydroxyl groups were outside the NPs, which was one reason of donor enrichment at the ETL interface. The intensity ratio of Cl to F in the blend films on PET- and $Zn(OAc)_2$-treated ZnO films was approximately 1.0,

https://doi.org/10.1021/acsami.1c02613
ACS Appl. Mater. Interfaces XXXX, XXX, XXX−XXX

which was lower than the cases of the pristine (1.6) and TMAH-treated ZnO (1.9) films. This result showed less enrichment of the polymer donor on top of the acid-treated ZnO films. For the inverted OSCs, electrons are transferred from acceptors to the ZnO ETL and collected by a cathode. Thus, the enrichment of donors at the cathode interface is not beneficial to charge transfer and collection. Therefore, the TOF-SIMS results confirmed the improved vertical phase separation with PET- and $Zn(OAc)_2$-treated ZnO ETLs, while TMAH treatment caused the opposite change. Meanwhile, an increased S content at the BHJ/ZnO interface was also observed in the PET-based film, proving that PET has been successfully attached to the top of the ZnO films.

The grazing incidence wide-angle X-ray scattering (GIWAXS) spectra of the blend films on different ZnO ETLs were studied and are shown in Figure 5a–d. The corresponding GIWAXS intensity profiles along the out-of-plane (OOP, black dotted line) and in-plane (IP, red dotted line) directions are shown in Figure 5e. The results were analyzed according to refs 61 and 62. The blend films on different ZnO ETLs showed similar features in the IP direction with the (100) lamellar stacking peak of ~0.309 $Å^{-1}$ (d = 20.33 Å) and in the OOP direction with the (010) $\pi-\pi$ stacking peak of ~1.75 $Å^{-1}$ (d = 3.59 Å), which were similar to the values in previous reports.[46] The crystal coherence length (CCL) values derived from the OOP (010) scattering for the blend films on top of the pristine and TMAH-, $Zn(OAc)_2$-, and PET-treated ZnO films are 18.1, 18.2, 19.0, and 18.3 Å, respectively. The CCL values of the (100) lamellar stacking in the IP direction are 91.9, 84.7, 98.8, and 93.7 Å, respectively. Also, the CCL values of OOP (100) scattering are 94.4, 87.8, 90.4, and 92.5 Å with the PM7:IT-4F films on top of these different ZnO films. These results suggested that the $Zn(OAc)_2$- and PET-treated ZnO ETLs have slight effects on the crystallinity of the blend films. On the TMAH-treated ZnO films, the smaller CCL of the lamellar stacking in the IP direction and $\pi-\pi$ stacking in the OOP direction indicated weaker crystallization propensity of the blend films.

After making sure that surface acid treatment has removed the surface OH groups, it was reasonable to speculate that the improvement of long-term stability after PET treatment might be also due to the removal of surface hydroxyl groups on the ZnO films. This speculation was strongly supported by the evolution of device efficiency when $Zn(OAc)_2$- and TMAH-treated ZnO films were used as ETLs. As shown in Figure S9, we found that the $Zn(OAc)_2$-treated device exhibited much slower degradation than the control device, while the device with the TMAH-treated ZnO ETL degraded much faster than the other solar cells. This observation clearly proved that the existence of a surface base has accelerated device degradation. The absorption of aged devices stored in a N_2-filled glove box under 100 h of continuous illumination was studied, and the absorption spectra of the films were slightly decreased compared to the fresh devices as shown in Figure S10, indicating the degradation of the organic layer. The absorption spectra of the ZnO/bulk heterojunction (BHJ) films and TMAH-, $Zn(OAc)_2$-, and PET-treated ZnO/BHJ films during continuous illumination were studied to gain deep insight into the deep mechanism. To clearly observe the evolution of the absorption spectra of the active layer, the thickness of the organic layer was controlled to be approximately 30 nm. As shown in Figure 6a–d, the pristine ZnO/PM7:IT-4F blend films exhibited typical absorption peaks at around 300, 600, and 750 nm, which were ascribed to the ZnO ETL, PM7 donor, and IT-4F acceptor, respectively.[63,64] During continuous illumination, the absorbance intensity of the ZnO and PM7 donor peaks did not show obvious degradation, while the absorbance peak of the IT-4F acceptor gradually decreased, suggesting degradation of the acceptor, which might be the main reason for device degradation. A similar degradation phenomenon was previously reported in NF acceptor-based OSCs, which has been ascribed to the chemical degradation of organic active materials at the interface of the ZnO ETL and organic layer due to the photocatalysis of ZnO films.[65] For the photocatalysis effect of ZnO, the process can be accelerated by hydroxyl groups;[66−68] therefore, a dramatic decrease in the acceptor absorbance peak was observed in the case of base-treated ZnO films. Particularly, after illumination for 49 h, the absorbance peak of IT-4F nearly disappeared in this film. Zhou *et al.* demonstrated that the NF acceptors are not stable in the base environment.[69] It is consistent with this work. In contrast, in the case of ZnO/$Zn(OAc)_2$/BHJ and ZnO/PET/BHJ films, the absorbance peaks of the active layer remained the same as the initial absorbance. These observations verified that surface weak treatment of the ZnO ETLs can effectively remove the surface hydroxyl groups and greatly suppressed the interface degradation, leading to significantly improved long-term stability. Meanwhile, it was a further proof that 2-phenylethylmercaptan did not chemically attack the donor or acceptor, although it is a good nucleophile and has a high chemical reactivity.

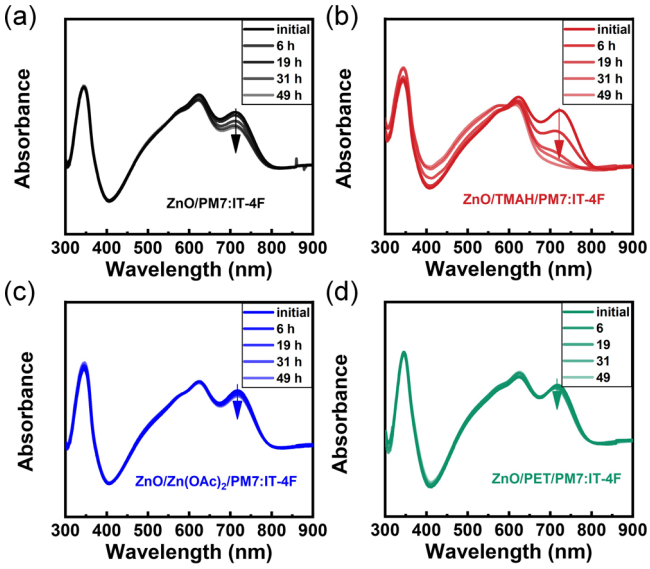

Figure 6. UV–vis absorbance spectra of the (a) ITO/ZnO/PM7:IT-4F, (b) ITO/ZnO/TMAH /PM7:IT-4F, (c) ITO/ZnO/$Zn(OAc)_2$/PM7:IT-4F, and (d) ITO/ZnO/PET/PM7:IT-4F films during continuous illumination.

Based on the above results, the working mechanism of ZnO surface acid treatment is illustrated in Figure 7. First, performance improvement resulted from the increase in J_{SC} and FF, which is due to the removal of surface recombination and a more favorable vertical component. For the pristine ZnO ETL-based solar cells, the hydroxyl ligands outside the ZnO NPs would act as recombination centers of free charge and decrease the current density. In addition, the stronger molecular interaction of ZnO and a polymer in the case of hydroxyl capping caused the obvious enrichment of polymer,

https://doi.org/10.1021/acsami.1c02613
ACS Appl. Mater. Interfaces XXXX, XXX, XXX−XXX

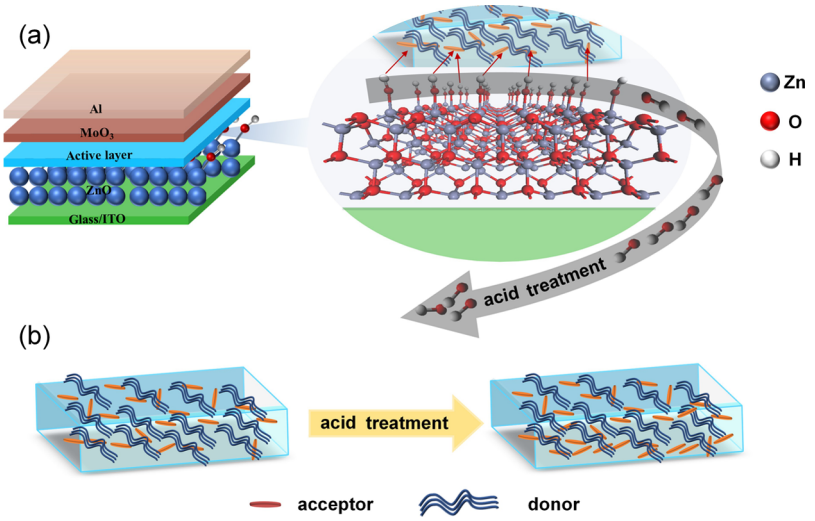

Figure 7. Schematic diagram of the mechanism of improved performance and stability with acid-treated ZnO films: (a) removal of surface OH groups on the surface of ZnO layers and (b) regulation of vertical phase separation in the heterojunction films.

which was another reason for the inferior device performance. Regarding the long-term stability, the excess hydroxyl groups would promote the photocatalytic effect of ZnO and hence accelerate the device degradation. The worsened degradation of the devices after treating the ZnO films with a base provided evidence of this conclusion. The strategy of simple surface treatment using various acids was effective because the surface hydroxyl groups were removed. Among these acids, the degradation of the organic layer in devices with PET-treated ZnO films was much slower than that in pristine ZnO film-based devices.

Finally, since the surface pH conditions of the ZnO ETLs are highly dependent on the synthesis conditions, it is noteworthy that significant improvements in the performance and stability were achieved through acid treatment of the ZnO films in the case of enormous hydroxyl groups surrounding the ZnO NPs. In the case of ZnO NPs with fewer surface hydroxyl groups, acid treatment of the ZnO films would show a slight impact on the improvement of the performance. Figure S11 shows the XPS spectra of a ZnO film with a lower defect oxygen ratio of 0.41. By using this ZnO as the ETL of the inverted solar cells, a reasonable performance with a PCE of 11.97% was achieved for PM7:IT-4F devices. PET treatment of the ZnO ETL led to less improvement of the PCE from 11.97 to 12.66% (as shown in Table S4, which is not as obvious as the result for the ZnO-based devices with high defect oxygen (as previously discussed)). Therefore, a conclusion could be made that acid treatment of the ZnO surface is an effective means to improve the OSC performance as long as unfavorable charge collection occurs because of adverse surface pH conditions. In the case of ZnO ETLs with fewer surface hydroxyl groups, surface acid treatment presented a weak improvement effect. Nevertheless, it is an effective, simple, and general method to solve the surface issue between the ZnO ETL and the active layer and ensure the high performance and long-term light stability of the NF OSCs.

4. CONCLUSIONS

In summary, we have investigated the effect of surface pH conditions on the device performance and stability of the NFA OSCs by treating the ZnO films with acids and bases. We found that base treatment caused poorer performance and accelerated the degradation of NFA OSCs, whereas simultaneous improvements in the efficiency and long-term stability of inverted NFA OSCs were achieved by treating the ZnO films with various acid solutions. Based on the film characterization, the existence of the enormous hydroxyl groups is the main reason for the inferior performance and stability. This occurs because the surface hydroxyl groups of the ZnO films cause interface recombination, lower the performance, and accelerate the photocatalytic process of the acceptor molecules, leading to rapid degradation of the nonfullerene acceptor at the ZnO/active layer interface. Among the different acid solutions, PET seems to be the most effective material. For PM7:IT-4F and PM6:Y6 solar cells, the PCE values were boosted from 10.95 to 13.19% and from 14.17 to 16.46%, respectively. The long-term stability was significantly improved (a T_{80} lifetime of over 4000 h) compared with pristine ZnO-based OSCs (a T_{80} lifetime of <10 h) for the PM6:Y6 devices. This work clearly showed the impact of surface pH conditions on the performance and stability of OSCs and provided a feasible approach to simultaneously improve the performance and stability of the NFA OSCs through surface acid treatment of ZnO ETLs. This work also showed the great potential of PM6:Y6 solar cells with high performance and long-term stability.

■ ASSOCIATED CONTENT

Supporting Information

The Supporting Information is available free of charge at https://pubs.acs.org/doi/10.1021/acsami.1c02613.

XRD patterns and TEM images of the ZnO nanoparticles and the absorbance spectra of the different ZnO films; $J-V$ characteristics of PM7:IT-4F solar cells during 10 min of light soaking with TMAH-treated ZnO as the ETL; T_{80} of the PM7:IT-4F and PM6:Y6 solar cells; dark $J-V$ characteristics, Nyquist plots, light intensity-dependent J_{SC} and V_{OC} of PM7:IT-4F devices with ZnO and PET-treated ZnO as ETLs; AFM images of different ZnO films; contact angle pictures of different ZnO films and PM7:IT-4F films; DFT simulation of the interaction effect; Nor-PCE decay curves of the devices

https://doi.org/10.1021/acsami.1c02613
ACS Appl. Mater. Interfaces XXXX, XXX, XXX−XXX

with different ZnO ETLs; absorbance spectra of the fresh and aged PM7:IT-4F devices; XPS spectra of the O 1s and Zn 2p core levels in the ZnO and PET-treated ZnO films with a lower ratio of vacancy oxygen to lattice oxygen; and additional tables (PDF)

AUTHOR INFORMATION

Corresponding Authors

Qun Luo − *School of Nano-Tech and Nano-Bionics, University of Science and Technology of China, Hefei 230027, P. R. China; Printable Electronics Research Center, Suzhou Institute of Nano-Tech and Nano-Bionics, Chinese Academy of Sciences (CAS), Suzhou 215123, P. R. China;* orcid.org/0000-0002-7527-460X; Email: qluo2011@sinano.ac.cn

Jianqi Zhang − *CAS Key Laboratory of Nanosystem and Hierarchical Fabrication, CAS Center for Excellence in Nanoscience, National Center for Nanoscience and Technology, Beijing 100190, P. R. China;* orcid.org/0000-0002-3549-1482; Email: zhangjq@nanoctr.cn

Chang-Qi Ma − *School of Nano-Tech and Nano-Bionics, University of Science and Technology of China, Hefei 230027, P. R. China; Printable Electronics Research Center, Suzhou Institute of Nano-Tech and Nano-Bionics, Chinese Academy of Sciences (CAS), Suzhou 215123, P. R. China;* orcid.org/0000-0002-9293-5027; Email: cqma2011@sinano.ac.cn

Authors

Yunfei Han − *School of Nano-Tech and Nano-Bionics, University of Science and Technology of China, Hefei 230027, P. R. China; Printable Electronics Research Center, Suzhou Institute of Nano-Tech and Nano-Bionics, Chinese Academy of Sciences (CAS), Suzhou 215123, P. R. China*

Huilong Dong − *School of Chemistry and Materials Engineering, Changshu Institute of Technology, Changshu 215500, P. R. China;* orcid.org/0000-0002-4436-6392

Wei Pan − *Printable Electronics Research Center, Suzhou Institute of Nano-Tech and Nano-Bionics, Chinese Academy of Sciences (CAS), Suzhou 215123, P. R. China*

Bowen Liu − *Printable Electronics Research Center, Suzhou Institute of Nano-Tech and Nano-Bionics, Chinese Academy of Sciences (CAS), Suzhou 215123, P. R. China*

Xingze Chen − *Printable Electronics Research Center, Suzhou Institute of Nano-Tech and Nano-Bionics, Chinese Academy of Sciences (CAS), Suzhou 215123, P. R. China*

Rong Huang − *Vacuum Interconnected Nanotech Workstation (Nano-X), Suzhou Institute of Nano-Tech and Nano-Bionics, Chinese Academy of Sciences (CAS), Suzhou 215123, P. R. China*

Zhiyun Li − *Vacuum Interconnected Nanotech Workstation (Nano-X), Suzhou Institute of Nano-Tech and Nano-Bionics, Chinese Academy of Sciences (CAS), Suzhou 215123, P. R. China*

Fangsen Li − *Vacuum Interconnected Nanotech Workstation (Nano-X), Suzhou Institute of Nano-Tech and Nano-Bionics, Chinese Academy of Sciences (CAS), Suzhou 215123, P. R. China*

Zhixiang Wei − *CAS Key Laboratory of Nanosystem and Hierarchical Fabrication, CAS Center for Excellence in Nanoscience, National Center for Nanoscience and Technology, Beijing 100190, P. R. China;* orcid.org/0000-0001-6188-3634

Complete contact information is available at: https://pubs.acs.org/10.1021/acsami.1c02613

Notes

The authors declare no competing financial interest.

ACKNOWLEDGMENTS

This work is financially supported by the National Natural Science Foundation of China (51773224 and 22075315), Youth Innovation Promotion Association, CAS (2019317), the Ministry of Science and Technology of China (2016 YFA0200700), and Vacuum Interconnected Nanotech Workstation, Suzhou Institute of Nano-Tech and Nano-Bionics, Chinese Academy of Sciences (CAS).

REFERENCES

(1) He, Z.; Xiao, B.; Liu, F.; Wu, H.; Yang, Y.; Xiao, S.; Wang, C.; Russell, T. P.; Cao, Y. Single-Junction Polymer Solar Cells with High Efficiency and Photovoltage. *Nat. Photonics* **2015**, *9*, 174−179.

(2) Han, Y.; Chen, X.; Wei, J.; Ji, G.; Wang, C.; Zhao, W.; Lai, J.; Zha, W.; Li, Z.; Yan, L.; Gu, H.; Luo, Q.; Chen, Q.; Chen, L.; Hou, J.; Su, W.; Ma, C.-Q. Efficiency above 12% for 1 cm^2 Flexible Organic Solar Cells with Ag/Cu Grid Transparent Conducting Electrode. *Adv. Sci.* **2019**, *6*, 1901490.

(3) Pan, W.; Han, Y. F.; Wang, Z. G.; Luo, Q.; Ma, C. Q.; Ding, L. M. Over 1 cm^2 Flexible Organic Solar Cells. *J. Semicond.* **2021**, *42*, 050301.

(4) Lin, Y.; Wang, J.; Zhang, Z. G.; Bai, H.; Li, Y.; Zhu, D.; Zhan, X. An Electron Acceptor Challenging Fullerenes for Efficient Polymer Solar Cells. *Adv. Mater.* **2015**, *27*, 1170−1174.

(5) Jiang, K.; Wei, Q.; Lai, J. Y. L.; Peng, Z.; Kim, H. K.; Yuan, J.; Ye, L.; Ade, H.; Zou, Y.; Yan, H. Alkyl Chain Tuning of Small Molecule Acceptors for Efficient Organic Solar Cells. *Joule* **2019**, *3*, 3020−3033.

(6) Liu, Q.; Jiang, Y.; Jin, K.; Qin, J.; Xu, J.; Li, W.; Xiong, J.; Liu, J.; Xiao, Z.; Sun, K.; Yang, S.; Zhang, X.; Ding, L. 18% Efficiency Organic Solar Cells. *Sci. Bull.* **2020**, *65*, 272−275.

(7) Lin, Y.; Nugraha, M. I.; Firdaus, Y.; Scaccabarozzi, A. D.; Aniés, F.; Emwas, A.-H.; Yengel, E.; Zheng, X.; Liu, J.; Wahyudi, W.; Yarali, E.; Faber, H.; Bakr, O. M.; Tsetseris, L.; Heeney, M.; Anthopoulos, T. D. A Simple n-Dopant Derived from Diquat Boosts the Efficiency of Organic Solar Cells to 18.3%. *ACS Energy Lett.* **2020**, *5*, 3663−3671.

(8) Yuan, J.; Zhang, Y.; Zhou, L.; Zhang, G.; Yip, H.-L.; Lau, T.-K.; Lu, X.; Zhu, C.; Peng, H.; Johnson, P. A.; Leclerc, M.; Cao, Y.; Ulanski, J.; Li, Y.; Zou, Y. Single-Junction Organic Solar Cell with over 15% Efficiency Using Fused-Ring Acceptor with Electron-Deficient Core. *Joule* **2019**, *3*, 1140−1151.

(9) Wang, F.; Tan, Z.; Li, Y. Solution-Processable Metal Oxides/Chelates as Electrode Buffer Layers for Efficient and Stable Polymer Solar Cells. *Energy Environ. Sci.* **2015**, *8*, 1059−1091.

(10) Krebs, F. C.; Thomann, Y.; Thomann, R.; Andreasen, J. W. A Simple Nanostructured Polymer/ZnO Hybrid Solar Cell-Preparation and Operation in air. *Nanotechnology* **2008**, *19*, 424013.

(11) Beek, W. J. E.; Wienk, M. M.; Kemerink, M.; Yang, X.; Janssen, R. A. J. Hybrid Zinc Oxide Conjugated Polymer Bulk Heterojunction Solar Cells. *J. Phys. Chem. B* **2005**, *109*, 9505−9516.

(12) Dkhil, S. B.; Duché, D.; Gaceur, M.; Thakur, A. K.; Aboura, F. B.; Escoubas, L.; Simon, J.-J.; Guerrero, A.; Bisquert, J.; Garcia-Belmonte, G.; Bao, Q.; Fahlman, M.; Videlot-Ackermann, C.; Margeat, O.; Ackermann, J. Interplay of Optical, Morphological, and Electronic Effects of ZnO Optical Spacers in Highly Efficient Polymer Solar Cells. *Adv. Energy Mater.* **2014**, *4*, 1400805.

(13) Sun, Y.; Seo, J. H.; Takacs, C. J.; Seifter, J.; Heeger, A. J. Inverted Polymer Solar Cells Integrated with A Low-Temperature-Annealed Sol-Gel-Derived ZnO Film as an Electron Transport Layer. *Adv. Mater.* **2011**, *23*, 1679−1683.

(14) Ma, Z.; Tang, Z.; Wang, E.; Andersson, M. R.; Inganäs, O.; Zhang, F. Influences of Surface Roughness of ZnO Electron

Transport Layer on the Photovoltaic Performance of Organic Inverted Solar Cells. *J. Phys. Chem. C* **2012**, *116*, 24462−24468.
(15) Qian, L.; Zheng, Y.; Xue, J.; Holloway, P. H. Stable and Efficient Quantum-Dot Light-Emitting Diodes based on Solution-Processed Multilayer Structures. *Nat. Photonics* **2011**, *5*, 543−548.
(16) Wu, B.; Wu, Z.; Yang, Q.; Zhu, F.; Ng, T. W.; Lee, C. S.; Cheung, S. H.; So, S. K. Improvement of Charge Collection and Performance Reproducibility in Inverted Organic Solar Cells by Suppression of ZnO Subgap States. *ACS Appl. Mater. Interfaces* **2016**, *8*, 14717−14724.
(17) Chen, S.; Small, C. E.; Amb, C. M.; Subbiah, J.; Lai, T.-h.; Tsang, S.-W.; Manders, J. R.; Reynolds, J. R.; So, F. Inverted Polymer Solar Cells with Reduced Interface Recombination. *Adv. Energy Mater.* **2012**, *2*, 1333−1337.
(18) Lee, B. R.; Jung, E. D.; Nam, Y. S.; Jung, M.; Park, J. S.; Lee, S.; Choi, H.; Ko, S. J.; Shin, N. R.; Kim, Y. K.; Kim, S. O.; Kim, J. Y.; Shin, H. J.; Cho, S.; Song, M. H. Amine-Based Polar Solvent Treatment for Highly Efficient Inverted Polymer Solar Cells. *Adv. Mater.* **2014**, *26*, 494−500.
(19) Polydorou, E.; Sakellis, I.; Soultati, A.; Kaltzoglou, A.; Papadopoulos, T. A.; Briscoe, J.; Tsikritzis, D.; Fakis, M.; Palilis, L. C.; Kennou, S.; Argitis, P.; Falaras, P.; Davazoglou, D.; Vasilopoulou, M. Avoiding Ambient Air and Light Induced Degradation in High-Efficiency Polymer Solar Cells by the Use of Hydrogen-Doped Zinc Oxide as Electron Extraction Material. *Nano Energy* **2017**, *34*, 500−514.
(20) Bai, S.; Jin, Y.; Liang, X.; Ye, Z.; Wu, Z.; Sun, B.; Ma, Z.; Tang, Z.; Wang, J.; Würfel, U.; Gao, F.; Zhang, F. Ethanedithiol Treatment of Solution-Processed ZnO Thin Films: Controlling the Intragap States of Electron Transporting Interlayers for Efficient and Stable Inverted Organic Photovoltaics. *Adv. Energy Mater.* **2015**, *5*, 1401606.
(21) Fu, P.; Guo, X.; Zhang, B.; Chen, T.; Qin, W.; Ye, Y.; Hou, J.; Zhang, J.; Li, C. Achieving 10.5% Efficiency for Inverted Polymer Solar Cells by Modifying the ZnO Cathode Interlayer with Phenols. *J. Mater. Chem. A* **2016**, *4*, 16824−16829.
(22) Zhu, X.; Guo, B.; Fang, J.; Zhai, T.; Wang, Y.; Li, G.; Zhang, J.; Wei, Z.; Duhm, S.; Guo, X.; Zhang, M.; Li, Y. Surface Modification of ZnO Electron Transport Layers with Glycine for Efficient Inverted Non-Fullerene Polymer Solar Cells. *Org. Electron.* **2019**, *70*, 25−31.
(23) Hau, S. K.; Yip, H.-L.; Ma, H.; Jen, A. K. Y. High Performance Ambient Processed Inverted Polymer Solar Cells through Interfacial Modification with A Fullerene Self-assembled Monolayer. *Appl. Phys. Lett.* **2008**, *93*, 233304.
(24) Stubhan, T.; Salinas, M.; Ebel, A.; Krebs, F. C.; Hirsch, A.; Halik, M.; Brabec, C. J. Increasing the Fill Factor of Inverted P3HT:PCBM Solar Cells Through Surface Modification of Al-Doped ZnO via Phosphonic Acid-Anchored C_{60} SAMs. *Adv. Energy Mater.* **2012**, *2*, 532−535.
(25) Park, S.; Son, H. J. Intrinsic Photo-Degradation and Mechanism of Polymer Solar Cells: the Crucial Role of Non-Fullerene Acceptors. *J. Mater. Chem. A* **2019**, *7*, 25830−25837.
(26) Ji, G.; Zhao, W.; Wei, J.; Yan, L.; Han, Y.; Luo, Q.; Yang, S.; Hou, J.; Ma, C.-Q. 12.88% Efficiency in Doctor-Blade Coated Organic Solar Cells through Optimizing the Surface Morphology of a ZnO Cathode Buffer Layer. *J. Mater. Chem. A* **2019**, *7*, 212−220.
(27) Jiang, Y.; Sun, L.; Jiang, F.; Xie, C.; Hu, L.; Dong, X.; Qin, F.; Liu, T.; Hu, L.; Jiang, X.; Zhou, Y. Photocatalytic Effect of ZnO on the Stability of Nonfullerene Acceptors and its Mitigation by SnO_2 for Nonfullerene Organic Solar Cells. *Mater. Horiz.* **2019**, *6*, 1438−1443.
(28) Liu, H.; Liu, Z. X.; Wang, S.; Huang, J.; Ju, H.; Chen, Q.; Yu, J.; Chen, H.; Li, C. Z. Boosting Organic−Metal Oxide Heterojunction via Conjugated Small Molecules for Efficient and Stable Nonfullerene Polymer Solar Cells. *Adv. Energy Mater.* **2019**, *9*, 1900887.
(29) Xu, X.; Xiao, J.; Zhang, G.; Wei, L.; Jiao, X.; Yip, H.-L.; Cao, Y. Interface-Enhanced Organic Solar Cells with Extrapolated T_{80} Lifetimes of over 20 Years. *Sci. Bull.* **2020**, *65*, 208−216.
(30) Cheng, H.-W.; Raghunath, P.; Wang, K.-l.; Cheng, P.; Haung, T.; Wu, Q.; Yuan, J.; Lin, Y.-C.; Wang, H.-C.; Zou, Y.; Wang, Z.-K.; Lin, M. C.; Wei, K.-H.; Yang, Y. Potassium-Presenting Zinc Oxide Surfaces Induce Vertical Phase Separation in Fullerene-Free Organic Photovoltaics. *Nano Lett.* **2020**, *20*, 715−721.
(31) Qian, L.; Zheng, Y.; Choudhury, K. R.; Bera, D.; So, F.; Xue, J.; Holloway, P. H. Electroluminescence from Light-Emitting Polymer/ZnO Nanoparticle Heterojunctions at Sub-Bandgap Voltages. *Nano Today* **2010**, *5*, 384−389.
(32) Trost, S.; Zilberberg, K.; Behrendt, A.; Polywka, A.; Görrn, P.; Reckers, P.; Maibach, J.; Mayer, T.; Riedl, T. Overcoming the "Light-Soaking" Issue in Inverted Organic Solar Cells by the Use of Al:ZnO Electron Extraction Layers. *Adv. Energy Mater.* **2013**, *3*, 1437−1444.
(33) Wei, J.; Ji, G.; Zhang, C.; Yan, L.; Luo, Q.; Wang, C.; Chen, Q.; Yang, J.; Chen, L.; Ma, C.-Q. Silane-Capped ZnO Nanoparticles for Use as the Electron Transport Layer in Inverted Organic Solar Cells. *ACS Nano* **2018**, *12*, 5518−5529.
(34) Pan, F.; Sun, C.; Li, Y.; Tang, D.; Zou, Y.; Li, X.; Bai, S.; Wei, X.; Lv, M.; Chen, X.; Li, Y. Solution-Processable n-Doped Graphene-Containing Cathode Interfacial Materials for High-Performance Organic Solar Cells. *Energy Environ. Sci.* **2019**, *12*, 3400−3411.
(35) Zeng, M.; Wang, X.; Ma, R.; Zhu, W.; Li, Y.; Chen, Z.; Zhou, J.; Li, W.; Liu, T.; He, Z.; Yan, H.; Huang, F.; Cao, Y. Dopamine Semiquinone Radical Doped PEDOT:PSS: Enhanced Conductivity, Work Function and Performance in Organic Solar Cells. *Adv. Energy Mater.* **2020**, *10*, 2000743.
(36) Yang, K.; Chen, S.; Fu, J.; Jung, S.; Ye, J.; Kan, Z.; Hu, C.; Yang, C.; Xiao, Z.; Lu, S.; Sun, K. Molecular Lock Induced by Chloroplatinic Acid Doping of PEDOT:PSS for High-Performance Organic Photovoltaics. *ACS Appl. Mater. Interfaces* **2020**, *12*, 30954−30961.
(37) Bai, Y.; Zhao, C.; Zhang, S.; Zhang, S.; Yu, R.; Hou, J.; Tan, Z.; Li, Y. Printable SnO_2 Cathode Interlayer with up to 500 nm Thickness-Tolerance for High-Performance and Large-Area Organic Solar Cells. *Sci. China. Chem.* **2020**, *63*, 957−965.
(38) Zhang, Z.; Zhang, Z.; Yu, Y.; Zhao, B.; Li, S.; Zhang, J.; Tan, S. Non-Conjugated Polymers as Thickness-Insensitive Electron Transport Materials in High-Performance Inverted Organic Solar Cells. *J. Energy Chem.* **2020**, *47*, 196−202.
(39) Zhu, L.; Zhang, M.; Zhou, G.; Hao, T.; Xu, J.; Wang, J.; Qiu, C.; Prine, N.; Ali, J.; Feng, W.; Gu, X.; Ma, Z.; Tang, Z.; Zhu, H.; Ying, L.; Zhang, Y.; Liu, F. Efficient Organic Solar Cell with 16.88% Efficiency Enabled by Refined Acceptor Crystallization and Morphology with Improved Charge Transfer and Transport Properties. *Adv. Energy Mater.* **2020**, *10*, 1904234.
(40) Gasparini, N.; Paleti, H. K.; Bertrandie, J.; Cai, G.; Zhang, G.; Wadsworth, A.; Lu, X.; Yip, H.-L.; McCulloch, I.; Baran, D. Exploiting Ternary Blends for Improved Photostability in High-Efficiency Organic Solar Cells. *ACS Energy Lett.* **2020**, *5*, 1371−1379.
(41) Yan, T.; Song, W.; Huang, J.; Peng, R.; Huang, L.; Ge, Z. 16.67% Rigid and 14.06% Flexible Organic Solar Cells Enabled by Ternary Heterojunction Strategy. *Adv. Mater.* **2019**, *31*, 1902210.
(42) Peng, R.; Yan, T.; Chen, J.; Yang, S.; Ge, Z.; Wang, M. Passivating Surface Defects of n-SnO_2 Electron Transporting Layer by InP/ZnS Quantum Dots: Toward Efficient and Stable Organic Solar Cells. *Adv. Electron. Mater.* **2020**, *6*, 1901245.
(43) Guang, S.; Yu, J.; Wang, H.; Liu, X.; Qu, S.; Zhu, R.; Tang, W. A Low Temperature Processable Tin Oxide Interlayer via Amine-Modification for Efficient and Stable Organic Solar Cells. *J. Energy Chem.* **2021**, *56*, 496−503.
(44) Bai, Y.; Zhao, C.; Shi, R.; Wang, J.; Wang, F.; Hayat, T.; Alsaedi, A.; Tan, Z. Novel Cathode Buffer Layer of $Al(acac)_3$ Enables Efficient, Large Area and Stable Semi-Transparent organic Solar Cells. *Mater. Chem. Front* **2020**, *4*, 2072−2080.
(45) Du, X.; Heumueller, T.; Gruber, W.; Almora, O.; Classen, A.; Qu, J.; He, F.; Unruh, T.; Li, N.; Brabec, C. J. Unraveling the Microstructure-Related Device Stability for Polymer Solar Cells Based on Nonfullerene Small-Molecular Acceptors. *Adv. Mater.* **2020**, *32*, 1908305.
(46) Fan, Q.; Zhu, Q.; Xu, Z.; Su, W.; Chen, J.; Wu, J.; Guo, X.; Ma, W.; Zhang, M.; Li, Y. Chlorine Substituted 2D-Conjugated Polymer

https://doi.org/10.1021/acsami.1c02613
ACS Appl. Mater. Interfaces XXXX, XXX, XXX−XXX

for High-Performance Polymer Solar Cells with 13.1% Efficiency via Toluene Processing. *Nano Energy* **2018**, *48*, 413−420.
(47) Upama, M. B.; Wright, M.; Mahmud, M. A.; Elumalai, N. K.; Mahboubi Soufiani, A.; Wang, D.; Xu, C.; Uddin, A. Photo-Degradation of High Efficiency Fullerene-Free Polymer Solar Cells. *Nanoscale* **2017**, *9*, 18788−18797.
(48) Cowan, S. R.; Roy, A.; Heeger, A. J. Recombination in Polymer-Fullerene Bulk Heterojunction Solar Cells. *Phys. Rev. B* **2010**, *82*, 245207.
(49) Koster, L. J. A.; Mihailetchi, V. D.; Xie, H.; Blom, P. W. M. Origin of the Light Intensity Dependence of the Short-circuit Current of Polymer/Fullerene Solar Cells. *Appl. Phys. Lett.* **2005**, *87*, 203502.
(50) Hawks, S. A.; Li, G.; Yang, Y.; Street, R. A. Band Tail Recombination in Polymer: Fullerene Organic Solar Cells. *J. Appl. Phys.* **2014**, *116*, 074503.
(51) Whelan, C. M.; Barnes, C. J.; Walker, C. G. H.; Brown, N. M. D. Benzenethiol Adsorption on Au(111) Studied by Synchrotron ARUPS, HREELS and XPS. *Surf. Sci.* **1999**, *425*, 195−211.
(52) Noh, J.; Ito, E.; Hara, M. Self-Assembled Monolayers of Benzenethiol and Benzenemethanethiol on Au(111): Influence of An Alkyl Spacer on the Structure and Thermal Desorption behavior. *J. Colloid Interface Sci.* **2010**, *342*, 513−517.
(53) Azmi, R.; Lee, C. L.; Jung, I. H.; Jang, S. Y. Simultaneous Improvement in Efficiency and Stability of Low-Temperature-Processed Perovskite Solar Cells by Interfacial Control. *Adv. Energy Mater.* **2018**, *8*, 1702934.
(54) Wilken, S.; Parisi, J.; Borchert, H. Role of Oxygen Adsorption in Nanocrystalline ZnO Interfacial Layers for Polymer-Fullerene Bulk Heterojunction Solar Cells. *J. Phys. Chem. C* **2014**, *118*, 19672−19682.
(55) Gong, Y.; Andelman, T.; Neumark, G. F.; O'Brien, S.; Kuskovsky, I. L. Origin of Defect-Related Green Emission from ZnO Nanoparticles: Effect of Surface Modification. *Nanoscale Res. Lett.* **2007**, *2*, 297−302.
(56) Bulliard, X.; Ihn, S. G.; Yun, S.; Kim, Y.; Choi, D.; Choi, J. Y.; Kim, M.; Sim, M.; Park, J. H.; Choi, W.; Cho, K. Enhanced Performance in Polymer Solar Cells by Surface Energy Control. *Adv. Funct. Mater.* **2010**, *20*, 4381−4387.
(57) Wang, J.; Zheng, Z.; Zhang, D.; Zhang, J.; Zhou, J.; Liu, J.; Xie, S.; Zhao, Y.; Zhang, Y.; Wei, Z.; Hou, J.; Tang, Z.; Zhou, H. Regulating Bulk-Heterojunction Molecular Orientations through Surface Free Energy Control of Hole-Transporting Layers for High-Performance Organic Solar Cells. *Adv. Mater.* **2019**, *31*, 1806921.
(58) Zheng, Z.; Zhang, S.; Wang, J.; Zhang, J.; Zhang, D.; Zhang, Y.; Wei, Z.; Tang, Z.; Hou, J.; Zhou, H. Exquisite Modulation of ZnO Nanoparticle Electron Transporting Layer for High-Performance Fullerene-Free Organic Solar Cell with Inverted Structure. *J. Mater. Chem. A* **2019**, *7*, 3570−3576.
(59) Owens, D. K.; Wendt, R. C. Estimation of the Surface Free Energy of Polymers. *J. Appl. Polym. Sci.* **1969**, *13*, 1741−1747.
(60) Angmo, D.; Andersen, T. R.; Bentzen, J. J.; Helgesen, M.; Søndergaard, R. R.; Jørgensen, M.; Carlé, J. E.; Bundgaard, E.; Krebs, F. C. Roll-to-Roll Printed Silver Nanowire Semitransparent Electrodes for Fully Ambient Solution-Processed Tandem Polymer Solar Cells. *Adv. Funct. Mater.* **2015**, *25*, 4539−4547.
(61) Müller-Buschbaum, P. The Active Layer Morphology of Organic Solar Cells Probed with Grazing Incidence Scattering Techniques. *Adv. Mater.* **2014**, *26*, 7692−7709.
(62) Jiang, X.; Kim, H.; Deimel, P. S.; Chen, W.; Cao, W.; Yang, D.; Yin, S.; Schaffrinna, R.; Allegretti, F.; Barth, J. V.; Schwager, M.; Tang, H.; Wang, K.; Schwartzkopf, M.; Roth, S. V.; Müller-Buschbaum, P. Internal Nanoscale Architecture and Charge Carrier Dynamics of Wide Bandgap Non-Fullerene Bulk Heterojunction Active Layers in Organic Solar Cells. *J. Mater. Chem. A* **2020**, *8*, 23628−23636.
(63) Zhao, W.; Li, S.; Yao, H.; Zhang, S.; Zhang, Y.; Yang, B.; Hou, J. Molecular Optimization Enables over 13% Efficiency in Organic Solar Cells. *J. Am. Chem. Soc.* **2017**, *139*, 7148−7151.
(64) Zhang, S.; Qin, Y.; Zhu, J.; Hou, J. Over 14% Efficiency in Polymer Solar Cells Enabled by a Chlorinated Polymer Donor. *Adv. Mater.* **2018**, *30*, 1800868.
(65) Qi, K.; Cheng, B.; Yu, J.; Ho, W. Review on the Improvement of the Photocatalytic and Antibacterial Activities of ZnO. *J. Alloys Compd.* **2017**, *727*, 792−820.
(66) Nguyen, H. T. P.; Nguyen, T. M. T.; Hoang, C. N.; Le, T. K.; Lund, T.; Nguyen, H. K. H.; Huynh, T. K. X. Characterization and Photocatalytic Activity of New Photocatalysts based on Ag, F-modified ZnO Nanoparticles Prepared by Thermal Shock Method. *Arab. J. Chem.* **2020**, *13*, 1837−1847.
(67) Cheng, C.; Amini, A.; Zhu, C.; Xu, Z.; Song, H.; Wang, N. Enhanced Photocatalytic Performance of TiO_2-ZnO Hybrid Nanostructures. *Sci. Rep.* **2014**, *4*, 04181.
(68) Ong, C. B.; Ng, L. Y.; Mohammad, A. W. A Review of ZnO Nanoparticles as Solar Photocatalysts: Synthesis, Mechanisms and Applications. *Renew. Sust. Energy Rev.* **2018**, *81*, 536−551.
(69) Zhu, X.; Hu, L.; Wang, W.; Jiang, X.; Hu, L.; Zhou, Y. Reversible Chemical Reactivity of Non-Fullerene Acceptors for Organic Solar Cells under Acidic and Basic Environment. *ACS Appl. Energy Mater.* **2019**, *2*, 7602−7608.

https://doi.org/10.1021/acsami.1c02613
ACS Appl. Mater. Interfaces XXXX, XXX, XXX−XXX